

Chapter 2

Lotus Versus Rose: Biomimetic Surface Effects

Michael Nosonovsky and Bharat Bhushan

Abstract The Lotus and rose petal effects have become a subject of active investigation by scientists, as they involve different modes of the interaction of wetting with roughness. The contact angle (CA) and CA hysteresis are two parameters, which characterize the hydrophobicity/philicity of a solid surface. Lotus-effect surfaces have a high CA and low CA hysteresis. However, it was found recently that a high CA can coexist with strong adhesion between water and a solid surface (and high CA hysteresis) in the case of the so-called “rose petal effect.” It is clear now that wetting cannot be characterized by only the CA, since several modes or regimes of wetting of a rough surface can exist, including the Wenzel, Cassie, Lotus, and Petal regimes. This is due to the hierarchical structure of rough surfaces built of micro- and nanoscale roughness, so that a composite interface can exist at the microscale, while a homogeneous interface can exist at the nanoscale or vice versa. The understanding of the wetting of rough surfaces is important in order to design non-adhesive surfaces for various applications, including environmental.

M. Nosonovsky
College of Engineering and Applied Science, University of Wisconsin,
Milwaukee, WI 53201, USA

B. Bhushan (✉)
Nanoprobe Laboratory for Bio- and Nanotechnology and Biomimetics (NLB2),
The Ohio State University, 201 W. 19th Avenue, Columbus,
OH 43210-1142, USA
e-mail: bhushan.2@osu.edu

2.1 Introduction

Wetting of rough surfaces is a complex problem which continues to attract scientists, in particular due to the emergence of new materials with controlled surface micro-, nano-, and hierarchical structure. During the past decade, the so-called “Lotus effect,” or surface roughness-induced superhydrophobicity and self-cleaning, became a subject of active investigation. According to early Wenzel [37] and Cassie and Baxter [9] models, there are two regimes of wetting of a rough surface: a homogeneous regime with a two-phase solid–water interface and a non-homogeneous or composite regime with a three phase solid–water–air interface (air pockets are trapped between the solid surface and water). Both models predict that surface roughness affects the water CA and can easily bring it to the extreme values close to 180° (superhydrophobicity) or close to 0° (superhydrophilicity). The studies of wetting of microstructured surfaces have concentrated on the investigation of the two regimes and the factors which affect the transition between the regimes [3, 5, 7, 16, 26–32].

Recent experimental findings and theoretical analyses made it clear that the early Wenzel [37] and Cassie and Baxter [9] models do not explain the complexity of interactions during wetting of a rough surface, which can follow several different scenarios [4, 5, 12, 14, 15, 22, 33, 36, 39]. As a result, there are several modes of wetting of a rough surface, and therefore, wetting cannot be characterized by a single number, such as the CA.

The concept of surface (or interface) energy is central for the analysis of wetting phenomena. Atoms or molecules at the surface of a solid or liquid have fewer bonds with neighboring atoms than those in the bulk. Energy is spent for breaking the bonds when a surface is created. As a result, the atoms at the surface have higher energy. This excess surface energy or surface tension, γ , is measured in N/m, and it is equal to the energy needed to create a surface with the unit area. If a liquid droplet is placed on a solid surface, the liquid and solid surfaces come together under equilibrium at a characteristic angle called the static CA, θ_0 , given by the Young equation [1, 2],

$$\cos \theta_0 = \frac{\gamma_{SA} - \gamma_{SL}}{\gamma_{LA}} \quad (2.1)$$

γ_{SL} , γ_{SA} , and γ_{LA} are the surface energies of the solid–liquid, solid–air, and liquid–air interfaces, respectively. For a large number of combinations of materials and liquids, $\gamma_{SA} + \gamma_{LA} > \gamma_{SL}$, which means that it is energetically profitable for a liquid to wet the solid surface rather than to have an air film separating the solid and liquid. On the other hand, for many material combinations, $\gamma_{SL} + \gamma_{LA} > \gamma_{SA}$, which means that it is energetically profitable for a solid to be in contact with air, rather than to be covered by a thin liquid film. As a result, in most situations $-1 < (\gamma_{SA} - \gamma_{SL})/\gamma_{LA} < 1$, and there exists a value of the CA given by Eq. 2.1. The CA is the angle under which the liquid–air interface comes in contact with the solid surface locally, and it does not depend on the shape of the body of water.

If water CA $0^\circ < \theta_0 < 90^\circ$, then the surface is usually called “hydrophilic,” whereas a surface with water CA $90^\circ < \theta_0 < 180^\circ$ is usually called “hydrophobic.”

In the ideal situation of a perfectly smooth and homogeneous surface, the static CA is a single number which corresponds to the unique equilibrium position of the solid–liquid–air contact line (the triple line). However, when the contact takes place with a rough surface, there may be multiple equilibrium positions which result in an entire spectrum of possible values of the CA. In addition, the value of the surface energy itself exhibits so-called “adhesion hysteresis” and can depend on whether it is measured during the approach of the two bodies or when they are taken apart. As the result, there is always the minimum value of the CA called the receding CA, θ_{rec} , and the maximum value of the CA called the advancing CA, θ_{adv} . The difference between the advancing and receding CA is called CA hysteresis (Fig. 2.1a).

Consider now a rough solid surface with the roughness factor $R_f > 1$ equal to the ratio of the solid surface area to its flat projected area. When water comes in contact with such a surface, the effective values of the solid–liquid and solid–air surface energies become $R_f \gamma_{\text{SL}}$ and $R_f \gamma_{\text{SA}}$ (Fig. 2.1b). This leads to the Wenzel equation for the CA with a rough surface [37]

$$\cos \theta = R_f \cos \theta_0 \quad (2.2)$$

If some air is trapped between the rough solid surface and the liquid, then only the fraction $0 < f_{\text{SL}} < 1$ constitutes the solid–liquid contact interface (Fig. 2.1c). The area of the solid–liquid interface is now $R_f f_{\text{SL}}$ per unit area, and in addition, there is $(1 - f_{\text{SL}})$ of the liquid–air interface under the droplet. The effective values of the solid–liquid and solid–air surface energies become $R_f f_{\text{SL}} \gamma_{\text{SL}}$ and $R_f f_{\text{SL}} \gamma_{\text{SA}} + (1 - f_{\text{SL}}) \gamma_{\text{LA}}$. The CA is then given by the Cassie and Baxter [9] equation

$$\cos \theta = R_f f_{\text{SL}} \cos \theta_0 - 1 + f_{\text{SL}} \quad (2.3)$$

If a surface is covered by holes filled (or impregnated) with water, the contact angle is given by

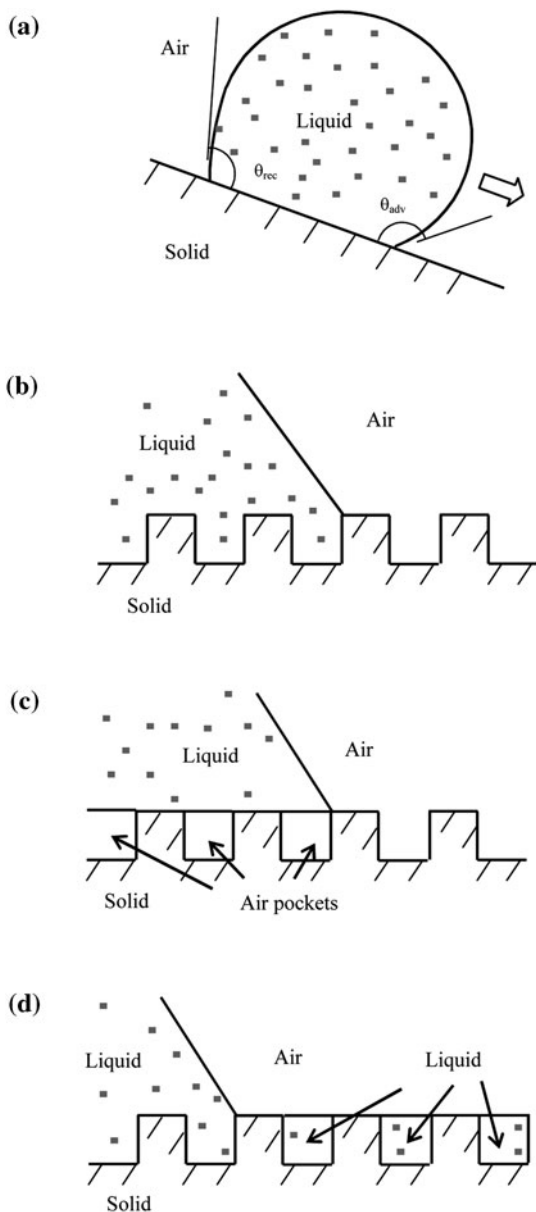
$$\cos \theta = 1 + f_{\text{SL}} (\cos \theta_0 - 1) \quad (2.4)$$

This is the so-called “impregnating” Cassie wetting regime [32] (Fig. 2.1d).

The CA is a macroscale parameter characterizing wetting. However, hydrophobicity/philicity is dependent upon the adhesion of water molecules to the solid. On the one hand, a high CA is a sign of low liquid–solid adhesion. On the other hand, low CA hysteresis is a sign of low liquid–solid adhesion as well. There is an argument in the literature as to whether superhydrophobicity is adequately characterized only by a high CA and whether a surface can have a high CA but at the same time strong adhesion. It is now widely believed that a surface can be superhydrophobic and at the same time strongly adhesive to water (e.g., [15]). The so-called “petal effect” is exhibited by a surface that has a high CA, but also a large CA hysteresis and strong adhesion to water. The phenomenon of the large

Fig. 2.1 **a** Schematics of a droplet on a tilted substrate showing advancing (θ_{adv}) and receding (θ_{rec}) contact angles. The difference between these angles constitutes the contact angle hysteresis.

Configurations described by **b** the Wenzel equation for the homogeneous interface, **c** Cassie–Baxter equation for the composite interface with air pockets, and **d** the Cassie equation for the homogeneous interface



CA hysteresis and high water adhesion to rose petals (and similar surfaces), as opposed to small CA hysteresis and low adhesion to Lotus leaf, was observed by several research groups [4, 8, 10]. Bormashenko et al. [8] reported a transition between wetting regimes, e.g., the penetration of liquid into the micro/nanostructures.

Li and Amirfazli [19] argued that since “superhydrophobicity” means a strong fear of water or lacking affinity to water, “the claim that a superhydrophobic surface also has a high adhesive force to water is contradictory.” Gao and McCarthy [14] pointed out that the terms “hydrophobic/phillic” should be defined in a more accurate way. They suggested several experiments showing that even Teflon[®], which is usually considered very hydrophobic, can be, under certain conditions, considered hydrophilic, i.e., has affinity to water. They argued that the concepts of “shear and tensile hydrophobicity” should be used, so that the wettability of a surface is characterized by two numbers, advancing and receding CAs, and “the words hydrophobic, hydrophilic, and their derivatives can and should only be considered qualitative or relative terms.” Instead, “shear and tensile hydrophobicity” should be investigated, which makes wetting (“solid–liquid friction”) similar to the friction force, as it has been pointed out in the literature earlier [23]. McHale [22] noted that all solid materials, including Teflon[®], are hydrophobic to some extent, if they have Young CA $< 180^\circ$. Therefore, it is energetically profitable for them to have contact with solid, at least to some extent. Wang and Jiang [36] suggested five superhydrophobic states (Wenzel’s state, Cassie’s state, so-called “Lotus” and “Gecko” states, and a transitional state between Wenzel’s and Cassie’s states). It may be useful also to see the transition between the Wenzel, Cassie, and dry states as a phase transition and to add the ability of a surface to bounce off a water droplet to the definition of the superhydrophobicity [31]. In addition, there is an argument on how various definitions of the CA hysteresis are related to each other [7, 8, 10, 17, 39]. A number of wetting regimes and transitions between them have been studied since 2010 [6, 11, 13, 34]. Modern research has concentrated on the ability to switch between the wetting states by tuning the surface energy [20, 21].

The Lotus effect has been comprehensively discussed in earlier publications. The objective of this paper is to discuss various wetting modes of rough surfaces, beyond the classical Wenzel [37] and Cassie and Baxter [9] regimes in light of recent experimental data on the petal effect and strong adhesion with superhydrophobic surfaces referred to as the “rose petal effect.”

2.2 Modeling CA Hysteresis

Predicting CA hysteresis for a rough surface with a given topography is a difficult task. One approach is a numerical simulation; however, in most cases the simulations are limited to two-dimensional (2D) topography. Kusumaatmaja and Yeomans [18] showed that contact angle hysteresis is sensitive to the details of the surface patterning. Despite that, certain conclusions about the relation of the contact angle hysteresis to roughness can be made. It is known that the energy gained for surfaces during contact is greater than the work of adhesion for separating the surfaces, due to so-called adhesion hysteresis. Factors that affect contact angle hysteresis include adhesion hysteresis, surface roughness, and

heterogeneity. Nosonovsky and Bhushan [26–29] assumed that contact angle hysteresis is equal to the adhesion hysteresis term and the term corresponding to the pinning effect of roughness, H_r . They further noted that the adhesion hysteresis can be assumed to be proportional to the fractional solid–liquid area ($1 - f_{LA}$). Using Eq. 2.3, the difference of cosines of the advancing and receding angles is related to the difference of those for a nominally smooth surface, θ_{adv0} and θ_{rec0} , as

$$\cos \theta_{adv} - \cos \theta_{rec} = R_f(1 - f_{LA})(\cos \theta_{adv0} - \cos \theta_{rec0}) + H_r \quad (2.5)$$

The first term in the right-hand part of the equation, which corresponds to the inherent contact angle hysteresis of a smooth surface, is proportional to the fraction of the solid–liquid contact area, $1 - f_{LA}$. The second term H_r is the effect of surface roughness, which is proportional to the length of the triple line. Thus Eq. 2.5 involves both the term proportional to the solid–liquid interface area and to the triple line length. It is observed from Eqs. 2.4 and 2.5 that increasing $f_{LA} \rightarrow 1$ results in increasing the contact angle ($\cos \theta \rightarrow -1$, $\theta \rightarrow \pi$) and decreasing the contact angle hysteresis ($\cos \theta_{adv} - \cos \theta_{rec} \rightarrow 0$). In the limiting case of a very small solid–liquid fractional contact area under the droplet, when the contact angle is large ($\cos \theta \approx -1 + (\pi - \theta)^2/2$, $\sin \theta \approx \theta - \pi$) and where the contact angle hysteresis is small ($\theta_{adv} \approx \theta \approx \theta_{rec}$), based on Eq. 2.5 [28],

$$\pi - \theta = \sqrt{2(1 - f_{LA})(R_f \cos \theta_0 + 1)} \quad (2.6)$$

$$\theta_{adv} - \theta_{rec} = (1 - f_{LA})R_f \frac{\cos \theta_{a0} - \cos \theta_{r0}}{-\sin \theta} = (\sqrt{1 - f_{LA}})R_f \frac{\cos \theta_{r0} - \cos \theta_{a0}}{\sqrt{2(R_f \cos \theta_0 + 1)}} \quad (2.7)$$

For the homogeneous interface, $f_{LA} = 0$, whereas for the composite interface f_{LA} is a non-zero number. It is observed from Eqs. 2.6–2.7 that for a homogeneous interface, increasing roughness (high R_f) leads to increasing the contact angle hysteresis (high values of $\theta_{adv} - \theta_{rec}$), while for a composite interface, an approach to unity of f_{LA} provides both high contact angle and small contact angle hysteresis [16, 26–28]. Therefore, the composite interface is desirable for self-cleaning.

A different semi-phenomenological model of the contact angle hysteresis has been proposed recently by Whyman et al. [38]. According to their model, the contact angle hysteresis is given by the equation $\theta_{adv} - \theta_{rec} = \left(\frac{8U}{\gamma R_0}\right)^{1/2} h(\theta^*)$, where U is the height of the potential barrier connected with the motion of the triple line along a substrate, R_0 is the initial radius of the spherical drop before deposition on the substrate, and $h(\theta^*)$ is the dimensionless function of the apparent contact angle θ^* .

Vedantam and Panchagunula [35] suggested a semi-empirical phase field method to calculate the CA hysteresis. In this method, the order-parameter $\eta(x, y)$ is selected in such a manner that $\eta = 0$ for the non-wetted regions of the surface and $\eta = 1$ for wetted regions, whereas $0 < \eta < 1$ for partially wetted regions. After that, the energy function $f(\eta)$ is constructed, and its minima correspond to the equilibrium states of the system (e.g., the Wenzel and Cassie states). After that, the energy functional is written as

$$L = \int_A \left\{ f(\eta) + \frac{\lambda}{2} |\nabla f(\eta)|^2 \right\} dA \quad (2.8)$$

where λ is the gradient coefficient. The functional that should be minimized involves the free energy and the gradient of the free energy. The latter term is needed to account for the fact that creating an interface between two phases is energetically unprofitable. The kinetic equation is given in the form

$$\beta \dot{\eta} = - \frac{dL}{d\eta} = \lambda \nabla^2 \eta - \frac{\partial f}{\partial \eta} \quad (2.9)$$

where $\beta > 0$ is the kinetic coefficient. Vedantam and Panchagunula [35] showed that in the case of $\beta = \text{const}$ for an axisymmetric drop flowing with the velocity V , Eq. 2.9 leads to

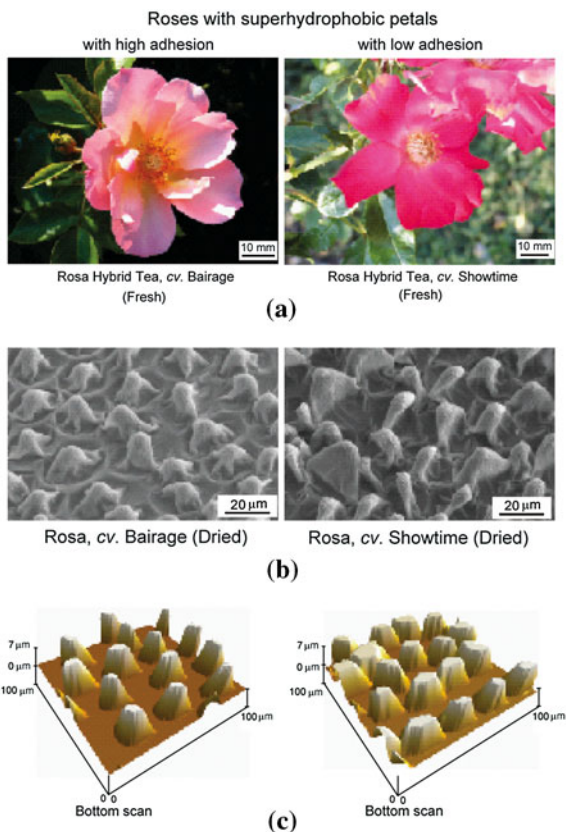
$$\cos \theta_{\text{adc}} - \cos \theta_{\text{rec}} = 2\alpha\beta V \quad (2.10)$$

In other words, assuming that the kinetic coefficient is constant, the contact angle hysteresis is expected to be proportional to the flow velocity. A more complicated form of the kinetic coefficient may lead to a more realistic dependence of the contact angle hysteresis on the velocity.

There is an asymmetry between the wetting and dewetting processes, since less energy is released during wetting than the amount required for dewetting due to adhesion hysteresis. Adhesion hysteresis is one of the reasons that leads to contact angle hysteresis, and it also results in the hysteresis of the Wenzel-Cassie state transition. The Cassie-Wenzel transition and CA hysteresis both may be considered as different manifestations of the same wetting–dewetting cycle behavior. Both the CA hysteresis and Cassie-Wenzel transition cannot be determined from the macroscale equations and are governed by micro- and nanoscale phenomena.

Note that the size of the surface roughness details is an important factor. It is generally assumed that the roughness factor R_f as well the fractional area of contact f_{SL} can be determined by averaging the surface roughness over some area, which is itself small relative to the size of the liquid droplet. For R_f and f_{SL} fractional areas changing with a spatial coordinate, special generalized Wenzel and Cassie equations, proposed by Nosonovsky [24], should be used. The size of the surface roughness also affects the ability of the interface to pin the triple line and thus affects the CA hysteresis. It could be claimed that CA hysteresis is a “second order” effect which is expected to vanish with the decreasing ratio of the size of

Fig. 2.2 **a** Optical images, **b** Scanning Microscope micrographs, and **c** Atomic Force Microscope roughness maps of petals of two roses [Rosa Hybrid Tea, cv. Bairage (Rosa, cv. Bairage), and Rosa Hybrid Tea, cv. Showtime (Rosa, cv. Showtime)] (adapted from [4])



the surface roughness and heterogeneity details to the droplet radius. This, however, does not happen since surface roughness and heterogeneity is an inherent property of any surface. There is a deep similarity between the dry friction and the wetting of a solid surface [23]. In the ideal situation of absolutely homogeneous and smooth surfaces there would be no friction and no CA hysteresis due to the absence of energy dissipation. However, in the real situations, surfaces are not ideal, and this leads to both dry friction and CA hysteresis. The development of quantitative relationships between the degrees of surface non-ideality (e.g., Shannon entropy of a rough surface) and CA hysteresis, remains an interesting task similar to the same task for friction [25].

2.3 Investigation of the Petal Effect

Plant leaves and petals provide an example of surfaces with high CA and high and low CA hystereses. Bhushan and Her [4] studied two kinds of superhydrophobic rose petals: (1) Rosa Hybrid Tea, cv. Bairage and (2) Rosa Hybrid Tea,

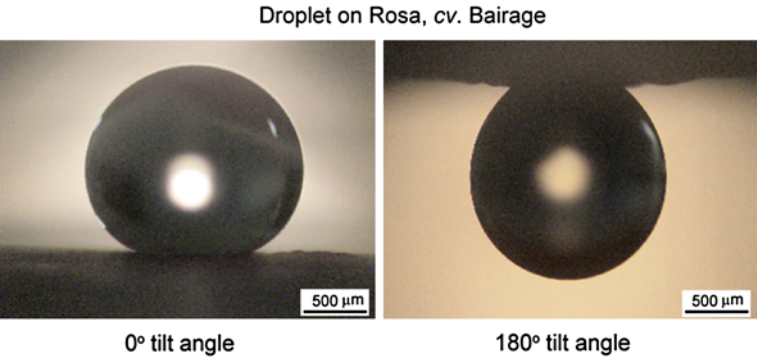


Fig. 2.3 Optical micrographs of water droplets on Rosa, cv. Bairage at 0° and 180° tilt angles. Droplet is still suspended when the petal is turned upside down [4]

Table 2.1 Surface roughness statistics for the two rose petals [4]

	Peak-to-base height (μm)	Midwidth (μm)	Peak radius (μm)	Bump density (1/10,000 μm ²)
Rosa, cv. Bairage (high adhesion)	6.8	16.7	5.8	23
Rosa, cv. Showtime (low adhesion)	8.4	15.3	4.8	34

Table 2.2 Wetting regimes of a surface with a single level of hierarchy of roughness

State	Cassie–Baxter	Wenzel	Impregnating cassie
Cavities	Air	Water under droplet	Water everywhere
CA	High	High	High
CA hysteresis	Low	Can be high	Low

cv. Showtime, referred to as Rosa, cv. Bairage and Rosa, cv. Showtime, respectively. Figure 2.2 shows optical micrographs and scanning electron microscopy (SEM) images and atomic force microscope (AFM) surface height maps of two rose petals. Figure 2.3 shows a sessile and a suspending water droplet on Rosa, cv. Bairage demonstrating that it can simultaneously have high CA and high adhesion and high CA hysteresis.

The surface roughness of the two rose petals was measured with the AFM, and the results for the peak-to-base height of bumps, the midwidth, peak radius, and bump density are summarized in Table 2.1. The data indicates that the low adhesion specimen (Rosa, cv. Showtime) has a higher density and height of the bumps, indicating that the penetration of water between the micro-bumps is less likely. Wetting of a rough surface with a single level of hierarchy of roughness details can follow several scenarios (Table 2.2).

Table 2.3 Different regimes of wetting of a surface with dual roughness

	Air in microstructure	Water under droplet in microstructure	Water impregnating microstructure
Air in nanostructure	Lotus, high CA, low CA hysteresis	Rose, high CA, high CA hysteresis	Rose filled microstructure
Water under droplet in nanostructure	Cassie (air-filled microstructure, water in nanostructure), high CA, low CA hysteresis	Wenzel (water in micro- and nanostructure), high CA, high or low CA hysteresis	Wenzel filled microstructure
Water impregnating nanostructure	Cassie filled nanostructure	Wenzel filled nanostructure	Wenzel filled micro and nanostructure

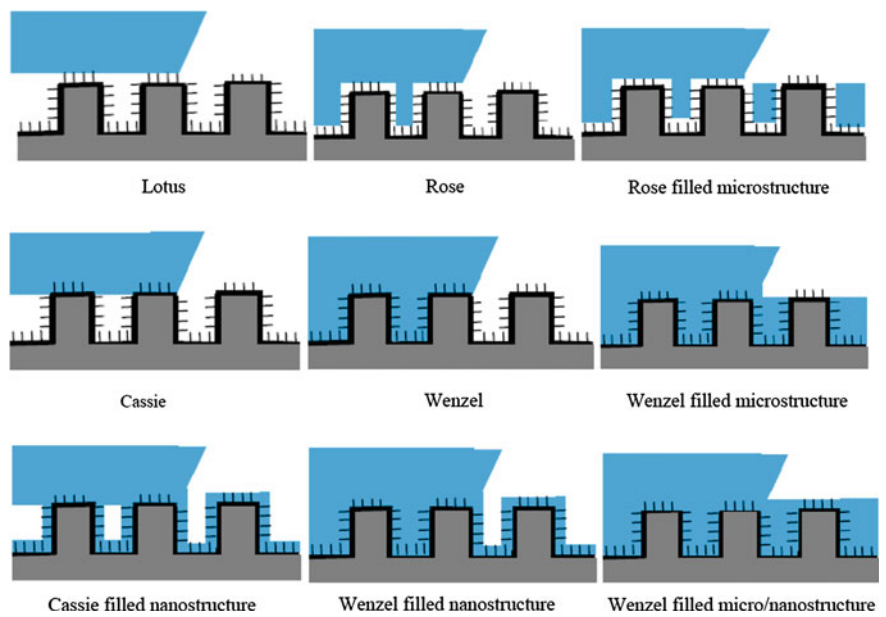


Fig. 2.4 Schematics of nine wetting scenarios for a surface with hierarchical roughness

For a hierarchical structure with small bumps on top of the larger bumps, a larger number of scenarios are available, and they are summarized in Table 2.3 and Fig. 2.4. Water can penetrate either in the micro- or nanostructure, or into both. In addition, the micro- or nanostructure can be impregnated by water or air. The regimes with water penetrating into the microstructure can have high solid–water adhesion and therefore high CA hysteresis.

Bhushan and Her [4] conducted a series of carefully designed experiments to decouple the effects of the micro- and nanostructures. They synthesized micro-structured surfaces with pillars out of epoxy resin. The epoxy surfaces were

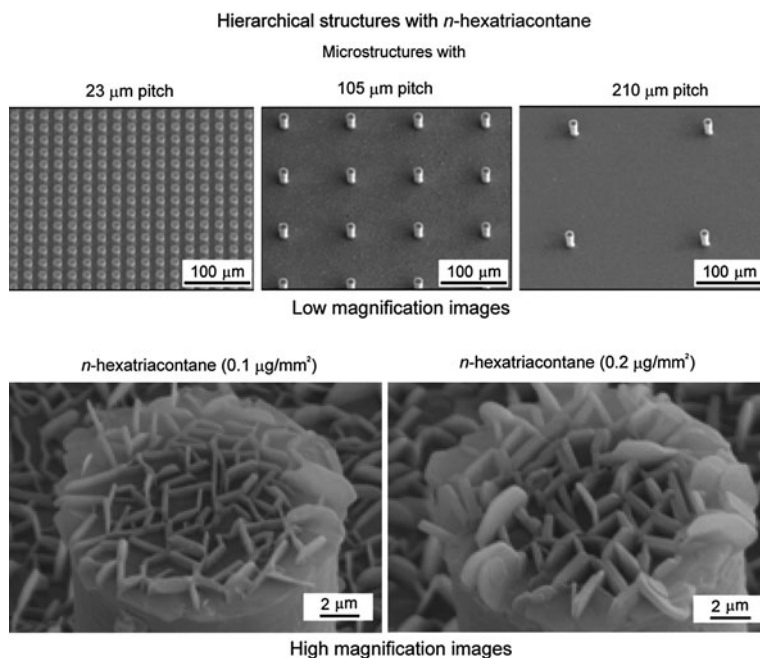


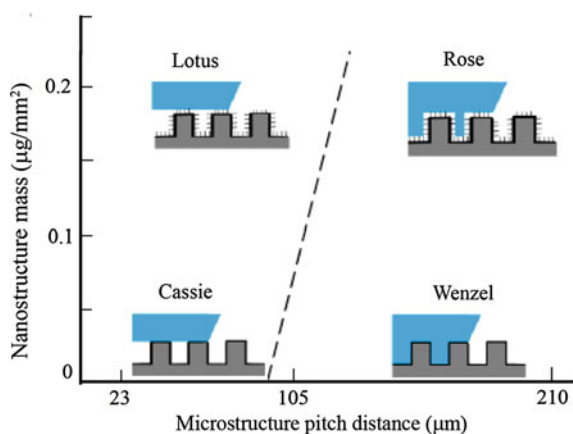
Fig. 2.5 SEM micrographs of the microstructures and nanostructures fabricated with two different masses of *n*-hexatriacontane for hierarchical structure. All images were taken at 45° tilt angle. All samples are positive replicas, obtained from negative replica with dental wax and Si micropatterned master template ($14\ \mu\text{m}$ diameter and $30\ \mu\text{m}$ height) fabricated with epoxy resin coated with *n*-hexatriacontane [4]

reproduced from model Si templates and were created by a two-step molding process producing a dual replica (first a negative replica and then a positive replica of the original Si template). Surfaces with a pitch (the periodicity of the structure of the pillars) of 23, 105, and $210\ \mu\text{m}$ and with the same diameter ($14\ \mu\text{m}$) and height ($30\ \mu\text{m}$) of the pillars were produced. After that, nanostructures were created on the microstructured sample by self-assembly of the alkane *n*-hexatriacontane ($\text{CH}_3(\text{CH}_2)_{34}\text{CH}_3$) deposited by a thermal evaporation method. Alkanes of varying chain lengths are common hydrophobic compounds of plant waxes. On smooth surfaces, alkanes can cause a large contact angle and a small contact angle hysteresis for water droplets. To fabricate the nanostructure, various masses of *n*-hexatriacontane were coated on a microstructure. The nanostructure is formed by three-dimensional platelets of *n*-hexatriacontane. Platelets are flat crystals, grown perpendicular to the surface. They are randomly distributed on the surface, and their shapes and sizes show some variation. Figure 2.5 shows selected images. When different masses of wax are applied, the density of the nanostructure is changed.

For surfaces with a small pitch of $23\ \mu\text{m}$, while the mass of *n*-hexatriacontane is changed, there are only small changes in the static contact angle and contact

Table 2.4 CA and CA hysteresis for surfaces with various micro- and nanoroughness (based on [4])

Mass of n-hexatriacontane ($\mu\text{g}/\text{mm}^2$)	Pitch					
	23 μm		105 μm		210 μm	
	CA	CA hysteresis	CA	CA hysteresis	CA	CA hysteresis
0.1	164°	3°	152	87	135	45
0.12	165°	3°	153	20	135	42
0.16	166°	3°	160	5	150	12
0.2	167°	3°	168	4	166	3

Fig. 2.6 Schematic of a wetting regime map as a function of microstructure pitch and the mass of nanostructure material. The mass of nanostructure material equal to zero corresponds to microstructure only (with the Wenzel and Cassie regimes). Higher mass of the nanostructure material corresponds to higher values of pitch, at which the transition occurs

angle hysteresis values, which means that they are always in the “Lotus” wetting regime. On the surface with a 210 μm pitch value, as the mass of n-hexatriacontane is increased, the static contact angle is increased, and the reverse trend was found for the contact angle hysteresis. This was interpreted as evidence that the nanostructure is responsible for the CA hysteresis and low adhesion between water and the solid surface. The results are summarized in Table 2.4. The wetting regimes are shown schematically in Fig. 2.6 as a function of the pitch of the microstructure and the mass of n-hexatriacontane. A small mass of the nanostructure material corresponds to the Cassie and Wenzel regimes, whereas a high mass of nanostructure corresponds to the Lotus and rose regimes. The Lotus regime is more likely for larger masses of the nanostructure material. Figure 2.7 shows a droplet on a horizontal surface of a hierarchical structure with 23 and 105 μm pitch and n-hexatriacontane (0.1 $\mu\text{g}/\text{mm}^2$). Air pockets are observed in the first case and not observed in the second case, indicating the difference between the two regimes [4].

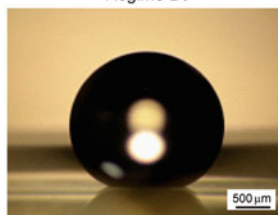
To further verify the effect of wetting states on the surfaces, evaporation experiments with a droplet on a hierarchical structure coated with two different

Fig. 2.7 **a** Droplet on a horizontal surface of hierarchical structure with 23 μm pitch and *n*-hexatriacontane ($0.1 \mu\text{g}/\text{mm}^2$) showing air pocket formation and **b** droplet on a hierarchical structure with 105 μm pitch and *n*-hexatriacontane ($0.1 \mu\text{g}/\text{mm}^2$) and $0.2 \mu\text{g}/\text{mm}^2$ showing no air pocket and air pocket formation, respectively. Also shown is the image taken on the inclined surface with hierarchical structure with $0.1 \mu\text{g}/\text{mm}^2$ showing that droplet is still suspended [4]

Shape of droplets on hierarchical structure with 23 μm pitch

Horizontal surface with *n*-hexatriacontane ($0.1 \mu\text{g}/\text{mm}^2$)

Regime B₁



(a)

Shape of droplets on hierarchical structure with 105 μm pitch

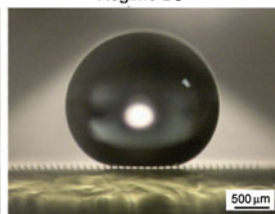
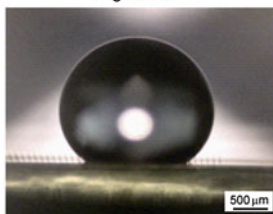
Horizontal surface with different mass of *n*-hexatriacontane

n-hexatriacontane ($0.1 \mu\text{g}/\text{mm}^2$)

n-hexatriacontane ($0.2 \mu\text{g}/\text{mm}^2$)

Regime A

Regime B₂

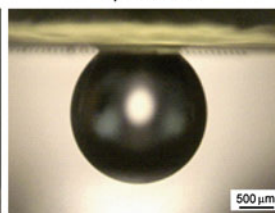
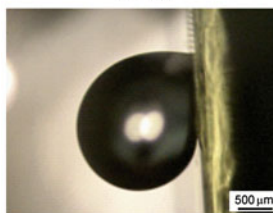


Inclined surface with *n*-hexatriacontane ($0.1 \mu\text{g}/\text{mm}^2$)

Regime A

vertical

upside down



(b)

amounts of *n*-hexatriacontane were performed. Figure 2.8 shows the optical micrographs of a droplet evaporating on two different hierarchical structured surfaces. On the *n*-hexatriacontane ($0.1 \mu\text{g}/\text{mm}^2$) coated surface, an air pocket was not visible at the bottom area of the droplet. However, the droplet on the surface has a high static contact angle (152°) since the droplet still cannot completely impregnate the nanostructure. The footprint size of the droplet on the surface has only small changes from 1820 to 1791 μm . During evaporation, the initial contact area between the droplet and hierarchical structured surface does not decrease until the droplet evaporates completely, which means complete wetting between droplet and microstructures. For the *n*-hexatriacontane ($0.2 \mu\text{g}/\text{mm}^2$) coated surface, the light passes below the droplet, and air pockets can be seen, so to start with the

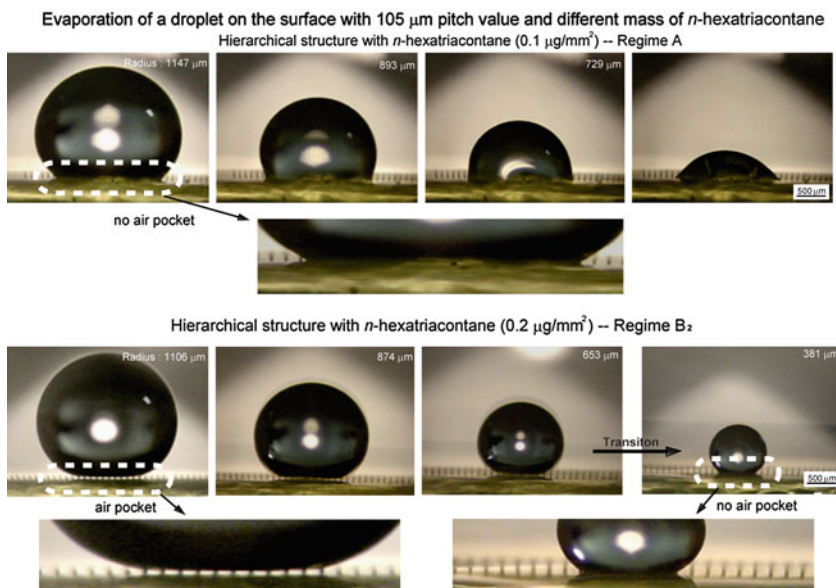


Fig. 2.8 Optical micrographs of droplet evaporation on the hierarchical structured surfaces with 105 μm pitch value. *n*-Hexatriacontane ($0.1 \mu\text{g}/\text{mm}^2$) coated sample has no air pocket formed between the pillars in the entire contact area until evaporation was completed. Hierarchical structure with *n*-hexatriacontane ($0.2 \mu\text{g}/\text{mm}^2$) has air pocket, and then the transition from the “Lotus” regime to the “Rose petal” regime occurred [4]

droplet is in the Cassie–Baxter regime. When the radius of the droplet decreased to 381 μm , the air pockets are not visible anymore. The footprint size of the droplet on the surface changed from 1177 to 641 μm , since droplet remained on only a few pillars until the end of the evaporation process.

The experimental observations of the two types of rose petals show that hierarchically structured plant surfaces can have both adhesive and non-adhesive properties at the same time with high CA. This is due to the existence of various modes of wetting of a hierarchical surface, so that water can penetrate either into macro- or nanoroughness, or into both. Water penetration into the microroughness tends to result in high adhesion with the solid surface, whereas the presence of the nanoroughness still provides high CA. As a result, two distinct modes of wetting are observed, one can be called the “Lotus” mode (with low adhesion) and the other is the “rose” mode with high adhesion.

2.4 Conclusions

In this work several modes of wetting of rough surfaces were investigated. Rose petals have different hierarchically organized surface micro- and nanostructures, and can exhibit high and low adhesion to water. The pitch spacing and height of

the microstructures controls the wetting regime, since it controls the penetration of water into the microstructure. The microstructure controls the CA hysteresis, whereas the nanostructure provides high CA. As a result, the rose petal can exhibit typical “Lotus effect” properties (high CA and low CA hysteresis) or “Petal effect” properties (high CA high CA hysteresis). Artificial surfaces which mimic rose petals were investigated and similar behavior found. Various wetting regimes are possible, depending on air and water penetration into the micro- and nano-structures. The understanding of the wetting of rough surfaces is important in order to design non-adhesive surfaces for various applications including green tribology.

Acknowledgment Michael Nosonovsky acknowledges the support of the UWM Research Growth Initiative grant.

References

1. B. Bhushan, *Principles and Applications of Tribology* (Wiley, New York, 1999)
2. B. Bhushan, *Introduction to Tribology* (Wiley, New York, 2002)
3. B. Bhushan, *Springer Handbook of Nanotechnology*, 3rd edn. (Springer, Heidelberg, 2010)
4. B. Bhushan, E.K. Her, Fabrication of superhydrophobic surfaces with high and low adhesion inspired from rose petal. *Langmuir* **26**, 8207–8217 (2010)
5. B. Bhushan, Y.C. Jung, Natural and biomimetic artificial surfaces for superhydrophobicity, self-cleaning, low adhesion, and drag reduction. *Prog. Mater. Sci.* **56**, 1–108 (2011)
6. B. Bhushan, M. Nosonovsky, The rose petal effect and the modes of superhydrophobicity. *Phil. Trans R. Soc. A* **368**, 4713–4728 (2010)
7. E. Bormashenko, Y. Bormashenko, T. Stein, G. Whyman, R. Pogreb, Z. Barkay, Environmental scanning electron microscope study of the fine structure of the triple line and cassie-wenzel wetting transition for sessile drops deposited on rough polymer substrates. *Langmuir* **23**, 4378–4382 (2007)
8. E. Bormashenko, T. Stein, R. Pogreb, D. Aurbach, “Petal effect” on surfaces based on lycopodium: high-stick surfaces demonstrating high apparent contact angles. *J. Phys. Chem. C* **113**, 5568–5572 (2009)
9. A. Cassie, S. Baxter, Wettability of porous surfaces. *Trans. Faraday Soc.* **40**, 546–551 (1944)
10. F.M. Chang, S.J. Hong, Y.J. Sheng, H.K. Tsao, High contact angle hysteresis of superhydrophobic surfaces: hydrophobic defects. *Appl. Phys. Lett.* **95**, 064102 (2009)
11. M.K. Dawood, H. Zheng, T.H. Liew, K.C. Leong, Y.L. Foo, R. Rajagopalan, S.A. Khan, W.K. Choi, Mimicking both petal and lotus effects on a single silicon substrate by tuning the wettability of nanostructured surfaces. *Langmuir* **27**, 4126–4133 (2011)
12. L. Feng, Y. Zhang, J. Xi, Y. Zhu, N. Wang, F. Xia, L. Jiang, Petal effect: a superhydrophobic state with high adhesive force. *Langmuir* **24**, 4114 (2008)
13. L. Feng, Y.A. Zhang, Y.Z. Cao, X.X. Ye, L. Jiang, The effect of surface microstructures and surface compositions on the wettabilities of flower petals. *Soft Matter* **7**, 2977–2980 (2011)
14. L. Gao, T.J. McCarthy, Teflon is hydrophilic. Comments on definitions of hydrophobic, shear versus tensile hydrophobicity, and wettability characterization. *Langmuir* **24**, 9184–9188 (2008)
15. M.H. Jin, X.L. Feng, L. Feng, T.L. Sun, J. Zhai, T.J. Li, L. Jiang, Superhydrophobic aligned polystyrene nanotube films with high adhesive force. *Adv. Mater.* **17**, 1977–1981 (2005)
16. Y.C. Jung, B. Bhushan, Contact angle, adhesion, and friction properties of micro- and nanopatterned polymers for superhydrophobicity. *Nanotechnology* **17**, 4970–4980 (2006)

17. B. Krasovitski, A. Marmur, Drops down the hill: theoretical study of limiting contact angles and the hysteresis range on a tilted plane. *Langmuir* **21**, 3881–3885 (2004)
18. H. Kusumaatmaja, J.M. Yeomans, Modeling contact angle hysteresis on chemically patterned and superhydrophobic surfaces. *Langmuir* **23**, 6019–6032 (2007)
19. W. Li, A. Amirfazli, Superhydrophobic surfaces: adhesive strongly to water? *Adv. Mater.* **19**, 3421–3422 (2007)
20. M.J. Liu, L. Jiang, Switchable adhesion on liquid/solid interfaces. *Adv. Func. Mater.* **20**, 3753–3764 (2010)
21. M.J. Liu, Y.M. Zheng, J. Zhai, L. Jiang, Bioinspired super-antiwetting interfaces with special liquid–solid adhesion. *Acc. Chem. Res.* **43**, 368–377 (2010)
22. G. McHale, All solids, including Teflon, are hydrophilic (to some extent), but some have roughness induced hydrophobic tendencies. *Langmuir* **25**, 7185–7187 (2009)
23. M. Nosonovsky, Model for solid–liquid and solid–solid friction for rough surfaces with adhesion hysteresis. *J. Chem. Phys.* **126**, 224701 (2007)
24. M. Nosonovsky, On the range of applicability of the wenzel and cassie equations. *Langmuir* **23**, 9919–9920 (2007)
25. M. Nosonovsky, Entropy in tribology: in search of applications. *Entropy* **12**, 1345–1390 (2010)
26. M. Nosonovsky, B. Bhushan, Biomimetic superhydrophobic surfaces: multiscale approach. *Nano Lett.* **7**, 2633–2637 (2007)
27. M. Nosonovsky, B. Bhushan, Multiscale friction mechanisms and hierarchical surfaces in nano- and bio-tribology. *Mater. Sci. Eng. R* **58**, 162–193 (2007)
28. M. Nosonovsky, B. Bhushan, Hierarchical roughness makes superhydrophobic surfaces stable. *Microelectron. Eng.* **84**, 382–386 (2007)
29. M. Nosonovsky, B. Bhushan, Hierarchical roughness optimization for biomimetic superhydrophobic surfaces. *Ultramicroscopy* **107**, 969–979 (2007)
30. M. Nosonovsky, B. Bhushan, Biologically-inspired surfaces: broadening the scope of roughness. *Adv. Func. Mater.* **18**, 843–855 (2008)
31. M. Nosonovsky, B. Bhushan, Energy transitions in superhydrophobicity: low adhesion, easy flow and bouncing. *J. Phys. Condens. Matter* **20**, 395005 (2008)
32. M. Nosonovsky, B. Bhushan, *Multiscale Dissipative Mechanisms and Hierarchical Surfaces: Friction, Superhydrophobicity, and Biomimetics* (Springer, Heidelberg, 2008)
33. M. Nosonovsky, B. Bhushan, Superhydrophobic surfaces and emerging applications: non-adhesion, energy, green engineering. *Curr. Opin. Colloid Interface Sci.* **14**, 270–280 (2010)
34. A. Tonosaki, T. Nishide, Novel petal effect of hafnia films prepared in an aqueous solution and containing hydroxy acids. *Appl. Phys. Express* **3**, 125801 (2010)
35. S. Vedantam, M.V. Panchagnula, Phase field modeling of hysteresis in sessile drops. *Phys. Rev. Lett.* **99**, 176102 (2007)
36. S. Wang, L. Jiang, Definition of superhydrophobic states. *Adv. Mater.* **19**, 3423–3424 (2007)
37. R.N. Wenzel, Resistance of solid surfaces to wetting by water. *Indust. Eng. Chem.* **28**, 988–994 (1936)
38. G. Whyman, E. Bormashenko, T. Stein, The rigorous derivation of young, cassie–baxter and wenzel equations and the analysis of the contact angle hysteresis phenomenon. *Chem. Phys. Lett.* **450**, 355–359 (2008)
39. F. Xia, L. Jiang, Bio-inspired, smart, multiscale interfacial materials. *Adv. Mater.* **20**, 2842–2858 (2008)

Green Tribology

Biomimetics, Energy Conservation and Sustainability

Nosonovsky, M.; Bhushan, B. (Eds.)

2012, XIV, 634 p., Hardcover

ISBN: 978-3-642-23680-8